TUDelft

Delft University of Technology

High Impedance Fault Detection using Advanced Distortion Detection Technique

Bhandia, Rishabh; de Jesus Chavez, Jose; Cvetkovic, Milos; Palensky, Peter

Important note
To cite this publication, please use the final published version (if applicable).
Please check the document version above.

High Impedance Fault Detection Using Advanced Distortion Detection Technique

Rishabh Bhandia , *Member, IEEE*, Jose de Jesus Chavez , *Member, IEEE*, Miloš Cvetković ,
and Peter Palensky , *Senior Member, IEEE*

Abstract—**A High Impedance Fault (HIF) in the power distribution systems remains mostly undetected by conventional protection schemes due to low fault currents. Apart from degrading the reliability of power supply to customers, HIF can impose a high cost on the utilities due to technical damages. The nonlinear and asymmetric nature of HIF makes its detection and identification very challenging. HIF signatures are in the form of minute-level distortions in the observable AC sinusoidal voltage and current waveforms but these signatures do not follow a clear pattern. In this paper, we present Advanced Distortion Detection Technique (ADDT), based on waveform analytics to distinguish and detect HIF. In addition, the ADDT analysis provides a fair assessment about the location and severity of HIF for efficient decision-making at the DSO level. ADDT is computationally lightweight and can be implemented in actual relays, hence it is enabled to provide an easy and cost-effective solution to HIF detection issues. ADDT robustness is tested in several simulation cases of interest using the IEEE-34 and IEEE-13 distribution test feeder systems in RTDS power system simulator. The test results successfully demonstrate the effectiveness and robustness of ADDT.**

Index Terms—**Advanced distortion detection technique, high impedance fault, power distribution system, power system protection, situational awareness, waveform analytics.**

I. Introduction

HIGH Impedance Faults (HIF) occur mostly in distribution systems. When a primary electrical conductor makes unwanted contact with high impedance objects like concrete, asphalt, sand or grass, it leads to a HIF generally characterized by arcing. Due to the high and nonlinear impedances of these objects, fault current drawn is very low. During this event, the fault current is not large enough to trigger the conventional protection schemes and thus HIF goes mostly undetected. According to the report compiled by Power System Relaying Committee (PSRC) [1], from the 200 HIF events staged over a period of time, only 35 were cleared by conventional protection systems.

HIF detection is further complicated by its unpredictable behavior. HIF do not follow a specific pattern which can be leveraged to detect them. Several studies have been conducted to identify defining characteristics of HIF in the voltage or current waveforms. Majority of these studies group HIF detection techniques in three main categories, the first two categories are domain-based, namely: time-domain and frequency-domain algorithms. The third category consists of techniques based on combining algorithms/tools to obtain the desired effect. Traditional time-domain based techniques used for HIF detection include the use of processing tools based on mathematical morphology to detect HIF [2], comparison of negative and positive current peaks to calculate current flicker and determine asymmetry in fault current [3], extracting signatures from current waveforms by observing change in ratio between substation and line ground resistances during HIF [4], ratio ground relaying based techniques [5], analyzing chaotic properties of HIF by fractal geometry techniques [6], transient analysis of disturbances to observe change in crest factor [7], profile identification of nonlinear voltage-current characteristics of HIF [8] and superimposition of voltage signals of certain frequencies to find HIF signatures [9]. Some of the traditional frequency-domain based techniques include monitoring of feeder current to find burst noise signal indicating HIF event [10], a range of algorithms based on lower order harmonics in [11]–[15]. The Fourier analysis based technique has been used in [16]. The techniques involving combination of domains include wavelet transform based techniques in [17]–[21]. Wavelet transformation along with pattern recognition has been used in [22], [23] to extract HIF features in order to detect them. The Kalman filtering based techniques have been used in [24], [25] to overcome certain shortcomings of Fourier analysis. The Pattern recognition based methods have been used exclusively in [26]–[28] to identify and conduct analysis of possible HIF specific features. Several learning techniques involving algorithms based on Artificial Neural Networks (ANN) have been used [29]–[32] to detect HIF. Several other HIF detection techniques found in [33]–[35] involve combination of multiple tools, but cannot be grouped under one common category of detection. An exhaustive study of the HIF detection techniques has been well documented in [36]. The above discussed techniques have been able to detect HIF with varying degree of success but many of them require extensive computing power, advanced learning algorithms or fault database which makes the implementation of these techniques

time-consuming, expensive and almost impossible to be implemented in actual field devices. Furthermore, with exception of [21], none of the techniques provide any estimate of how HIF event can be located based on detection results.

This paper proposes Advanced Distortion Detection Technique (ADDT) to accurately detect HIF while addressing the challenges faced by above discussed HIF detection techniques. The main added value of ADDT, when compared to previous literature, is that ADDT has extremely low computational burden, which makes it a fast and resourceful HIF detection technique. ADDT operates by leveraging the unique characteristics of pure AC sinusoid waveforms which means that neither does ADDT require complex learning algorithms nor the historical database of fault signatures. ADDT operates by first detecting current or voltage waveform distortions produced due to occurrence of any event in the grid. ADDT then uses distinctive indicators to assess the possible danger posed to the normal grid operations from the event and accordingly classifies the severity of the event on a specific scale proposed in this paper so that grid operators have a better understanding of the damage potential of the event. Based on the information from the indicators, ADDT also provides a fair idea about the location of the event. Since, any HIF event, regardless of its non-linearity or randomness, would also produce minute-level distortions in the sinusoid current or voltage waveforms, ADDT would analyze these minute distortions to detect HIF. ADDT's resourcefulness can be highlighted by the fact that it is straightforward to implement and it can be integrated on conventional protection devices to create a single multi-purpose Intelligent Electrical Device (IED) to tackle all protection issues in distribution grids.

In this paper we perform functional validity test of ADDT in context of HIF detection. ADDT presented in this paper follows from the preliminary work done by the same authors in waveform distortion detection [37] and evaluation of results against that of commercial relays [38]. In this paper we present a comprehensive study of ADDT performance in the presence of external factors to recreate realistic grid conditions. We demonstrate the ADDT's robustness and ability to detect and distinguish HIF in simulation cases of interest as explained in later sections. The study cases are simulated in IEEE-34 node and IEEE-13 node distribution feeder systems in real-time simulation environment using RTDS and the corresponding waveform analysis in MATLAB.

The details of ADDT and its various components are explained in Section II. Section III describes the standard HIF model and test systems used for simulations. Section IV presents the several simulations cases and scenarios chosen for ADDT implementation. Section V discusses the ADDT implementation results. Section VI presents the remarks and discussion on ADDT performance while Section VII presents the conclusions.

II. ADVANCED DISTORTION DETECTION TECHNIQUE

The ADDT implementation, as shows the flowchart in Fig. 1, comprises of five functional blocks. The sampled current or voltage measurement signals form the input to ADDT analysis. The measurement signals can be acquired from IEDs. The sampling
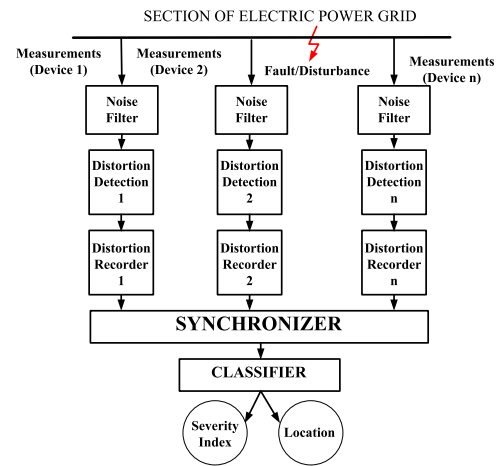

Fig. 1. ADDT Overview.

period of the signals is user dependent and should be based on the fidelity of the measurement device. ADDT however works best at high sampling rates (in the order of milliseconds).

The comprising functional blocks and their role are presented sequentially, from the acquisition of raw measurements for detecting detections and then using distinctive indicators for intelligent decision making for the operators.

A. Noise Filter

Noise can lead to distortion of waveforms thereby masking the event signature. Electrical noise in a power distribution network generally ranges from 5 kHz to 100 kHz [39]. ADDT implements a low pass Butterworth filter with cut off frequency at 2 kHz to remove any noise from the measured waveforms. The input to Noise Filter block is current or voltage waveform $f[k]$, measured with a sampling rate S from a specific measurement device in the grid.

B. Distortion Detection

Distortion Detection block forms the heart of the ADDT implementation. The definition of '*distortion*' and the theory of detecting a distortion are explained first followed by the implementation mechanism.

1) Definition and Theory: ADDT relies on the fact that current and voltage waveforms in an AC system are pure sinusoids under the ideal conditions (no distortions or noise) unless distorted by any event occurring in the grid. Complex exponentials like pure sinusoids exhibit few unique characteristics. The instance when these unique characteristics are violated, the waveform ceases to be a pure sinusoid at that instant and this occurrence is characterized as '*distortion*' in ADDT context.

Let us consider a waveform with no distortions (pure sinusoid). These pure sinusoids are complex exponential functions and can be represented by Euler's formula as:

$$e^{j\omega t} = \cos \omega t + \mathrm{j} \sin \omega t \qquad (1)$$

where ω is the angular frequency (*in radians per second*), t is time (seconds) and j is the imaginary unit.
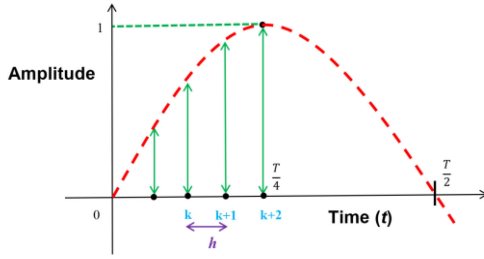
Fig. 2.   Sampled pure sinusoid signal *f[k]*.

One unique characteristic of complex exponentials is that the rate of increase or decrease of the function is proportional to the value of the function at that instant. Hence, the increase or decrease of the function can be analytically computed. Another unique characteristic is that complex exponentials are not infinitely increasing or decreasing. They always rotate around the unit circle in a complex plane. These above discussed characteristics form the bedrock of ADDT analysis, since the violation of either is an indication of a *distortion*. ADDT leverages these unique characteristics of complex exponentials to differentiate between pure and distorted sinusoids.

The mathematical formulation of ADDT is based on the distortion detection theory explained above. Let us consider a sampled pure sinusoid signal $f[k]$ as shown in Fig. 2. It is a general representation of any voltage or current signal measured from the grid.

Assuming the signal is a sine wave of period T, which can be sampled at N samples per cycle, the times when the samples are collected could be denoted as: $n, \ldots, k, k+1, k+2, \ldots, n+N$. The samples are equally spaced in time at an interval of length h, such that:

$$T = h \cdot N \tag{2}$$

Let $g[k]$ be the difference of the sampled values for samples k and $k+1$, the first difference at k can be written as:

$$g[k] = \frac{f[k] - f[k-1]}{h} \tag{3}$$

Similarly at $k+1$:

$$g[k+1] = \frac{f[k+1] - f[k]}{h} \tag{4}$$

For a pure sine wave, using (3) and (4), it can be written that:

$$g[k] > g[k+1], k \in \left\{n, n+\frac{T}{4}\right\} \cup \left\{n+\frac{T}{2}, n+\frac{3T}{4}\right\} \tag{5}$$

$$g[k] < g[k+1], k \in \left\{n+\frac{T}{4}, n+\frac{T}{2}\right\} \cup \left\{n+\frac{3T}{4}, n+T\right\} \tag{6}$$

Hence, if $f[k]$ is a pure sine wave, Equations (5) and (6) would always hold true. If these equations are violated under any circumstance, the violation will be recorded as a *distortion*. The low computational burden of Equations (3) and (4) makes ADDT lightweight and fast.

2) Implementation: The mathematical formulation of detection theory is programmed in the Distortion Detection block. The output of this block is a tuple (d, t) where d indicates the occurrence of the distortion at time t. If a distortion is detected, then d is defined as, $d = 1$ and if distortion is not detected, $d = 0$. This output serves as an input to the Distortion Recorder block.

C. Distortion Recorder

The distortions detected during real-time need to be stored temporarily in small time-frames of specified length for fast time-synchronization by the *Synchronizer* block and quick analysis by the *Classifier* block to achieve accurate decision-making.

The input data from distortion detection block is collected in a dataset called Memory Buffer. The last R samples are stored in the memory buffer. The size of the window is user-dependent and could vary from one measurement device to other. If we have m measuring devices such that $i = 1, 2, 3, \ldots, m$, then the memory buffer W_i in the time interval of (a_i, b_i) can be represented as:

$$W_i = \{(d_f, t_f) \,|\, d_f \in \{0,1\}, \; t_f \in (a_i, b_i), f$$
$$= (1, 2, 3, \ldots, N)\} \tag{7}$$

The memory buffer W_i contains the instants of occurrence and non-occurrence of distortions in a fixed length of time interval (a_i, b_i). Memory buffer W_i serves as an input to the synchronizer block.

D. Synchronizer

The measurement devices on the grid may not always have the same sampling rate. Hence, synchronization of memory buffer according to the time-stamp is a necessity to avoid incorrect detection. The device with highest sampling rate will have the greatest resolution and hence the smallest time-frame needed for the memory buffer. This smallest time-frame forms base window for synchronization. Base window A can be represented as:

$$A = (a_{base}, b_{base}) = \bigcap_{i=1}^{n} (a_i, b_i) \tag{8}$$

The curtailed memory buffer $\breve{W}_i$ within the size limits of the base window can be represented as:

$$\breve{W}_i = \{w_i = (d_f, t_f) \,|\, w_i \text{ and } t_f$$
$$\in (a_{base}, b_{base}) \text{ and } d_f \in \{0,1\}\} \tag{9}$$

The last processing step of this block is to sum the values of the distortion occurrences d_f in the time interval of the curtailed memory buffer $\breve{W}_i$, i.e.,:

$$C_i = \sum_{p=1}^{|\breve{W}_i|} d_p \tag{10}$$

The final output of the synchronizer block are time-synchronized datasets of the various measurement devices containing information regarding the total number of distortions detected in the time interval t_f.

TABLE I
SEVERITY RATING SCALE (BOTH LMD AND NT LEVEL)

Severity Rating Level	Interpretation	Possible Response
0	Normal Operation (Green Flag)	No intervention needed
1	Minimal Risk, some usual grid operations (Yellow Flag)	On alert, to keep checking for change in severity rating
2	Definite risk, unusual happenings (Orange Flag)	Plan adequate response and implement it
3	Major risk, fault occurrence imminent (Red Flag)	Implement quickest response possible

E. Classifier

The classifier block grades the distortion inducing event on a severity rating scale to reflect the extent of damage the event can cause. The concept of severity rating is necessitated by the fact that any event causing distortions will not have the same effect over the entire section of the grid. For the same event, some measurement devices may report numerous and frequent distortions, some comparatively lower and some may not report any distortion at all. Also, normal grid operations like load and capacitor switching might produce few distortions but they will not lead to any disruption or blackout. Hence, severity rating is needed to gauge the impact of the event at different points in grid and accordingly classify the severity of the event. Severity Rating can be further used to locate the event. Severity rating scale as shown in Table I also lists possible responses to the corresponding alert levels.

The severity rating scale is based on certain thresholds. These thresholds would be determined by calculating the percentage of distorted samples to total number of samples in one cycle. Severity rating moves up on the scale when the scale specific threshold is violated. Based on a number of empirical studies of distortions under normal grid events and conventional fault events at different locations in distribution grids, it is observed that in pure sinusoid (no distortions or noise), the percentage of distorted samples for normal grid operations are very low (<2%) while for conventional faults it can go up to 30% or more. Accordingly, the thresholds for Table I is determined with level 0 indicating <2% of distorted samples to around 15% distorted samples indicating level 3. The levels in-between are spaced out by 4% buffer. Hence for the severity rating to scale up from level 0 to level 1, 6% of the samples need to be distorted and so on. The severity rating scale and threshold determination is flexible and based on DSO requirements; it can be adjusted with additional alert levels and responses.

We propose to allocate severity rating on two levels. The first is the Local Measurement Device (LMD) level to rate the *intensity of the event* at the place of measurement. This severity rating is allocated for a specific measurement device based on the distortions the device has detected. The second is the Network (NT) level (comprising analysis of cumulated data from all measurement devices) to rate the *impact of the event*. This severity rating is allocated based on number of common distortions detected by all measurement devices. The proposed severity rating scale for both LMD and NT level is same as shown in Table I.

Severity rating allocation on both levels is further based on two distinctive indicators.

a) **Time-Frame:** This is the minimum time-interval after which the severity rating is re-assessed based on the number of distorted samples detected in that interval. The time-frame is user dependent. The time frame remains the same for severity rating at both LMD and NT levels.

b) **Number of Distortions Reported:** A normal switching case will produce few distortions while a fault inducing event will cause multiple distortions over time. This indicator is implemented differently for LMD and NT levels. In the LMD level, based on the number of distortion recorded in a particular time-frame by a specific measurement device, a LMD specific severity rating is allocated. However in case of NT level, the concept of Common Reporting's is introduced. The time stamped synchronized dataset from Synchronizer block can indicate how many measurement devices are reporting distortions at the same time (Common Reporting's). This helps the classifier to gauge the impact of the event across the network or a section of network and accordingly assign an NT level severity rating.

This two tier severity rating system also helps in tracing the location of the event. The LMD level severity reporting identifies measurement devices reporting highest severity rating. Hence, one can conclude that the event is possibly located between the areas covered by the measurement devices reporting highest severity rating. Based on these observations the maintenance team can focus on locating the exact event location in a span of a relatively smaller area compared to the entire spread of the distribution grid leading to better utilization of time and resources.

ADDT analysis results are meant to be relayed to the grid operator at DSO level. ADDT analysis including the two tier severity rating will help the grid operator to have a better situational awareness of the grid operations. DSO's can then choose from several possible responses and fix the problem affecting the grid before it possibly cascades into a blackout. The ADDT implementation flowchart can be seen in Fig. 3.

III. SIMULATION MODELS

In this section, we describe the HIF model and the test system used for the simulations.

A. HIF Model

In this paper, the standard HIF model from [2] has been adapted and remodeled in the Real Time Digital Simulator (RTDS). The model in [2] is an adaptation of a staged HIF event in [3]. The modeling is done to include typical HIF current characteristics as: buildup, shoulder, asymmetry, nonlinearity, and intermittence as explained in [21]:

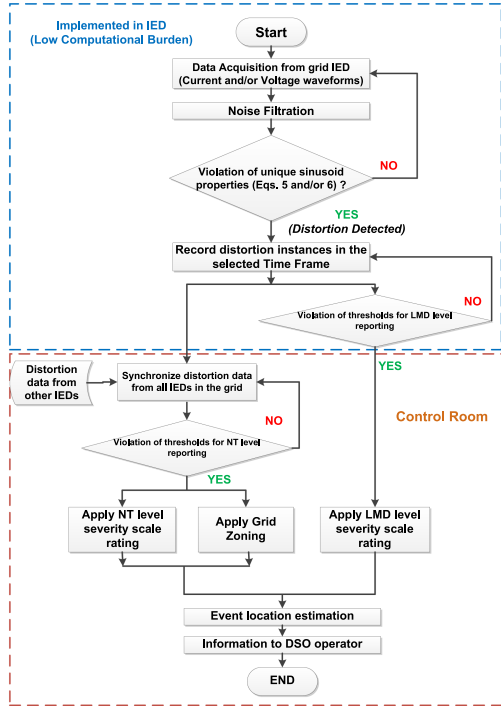1) Buildup: The gradual increase of the current amplitude to its maximum.
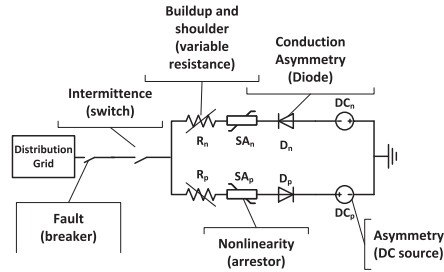
Fig. 3.   ADDT implementation flowchart.

Fig. 4.   HIF model (RSCAD).

2) Shoulder: The period in which the buildup stops and current amplitude remains constant.

3) Asymmetry: Fault current having different random peak values for positive and negative half-cycles.

4) Nonlinearity: Current value changes randomly from cycle to cycle resulting in a nonlinear voltage-current characteristic curve.

5) Intermittence: The time period of arcing between two bursts.

The HIF model shown in Fig. 4 consists of two DC sources (DC_N and DC_P) whose magnitudes are different from each other to produce the magnitude asymmetry between the positive and negative half-cycles. The DC sources are connected to a pair of diodes (D_N and D_P) that produce an asymmetric conductance due to voltage differences in their terminals. The diodes are connected to a pair of surge arrestors (SA_p and SA_n), which are responsible for producing the nonlinear characteristics. The surge arrestors are connected in turn to time variant resistances (R_p and R_n). The magnitude of such time-variant resistances is varied to create the buildup and shoulder characteristics similar
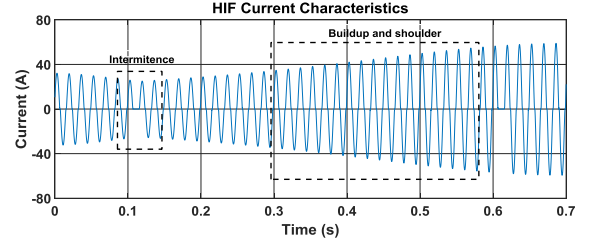

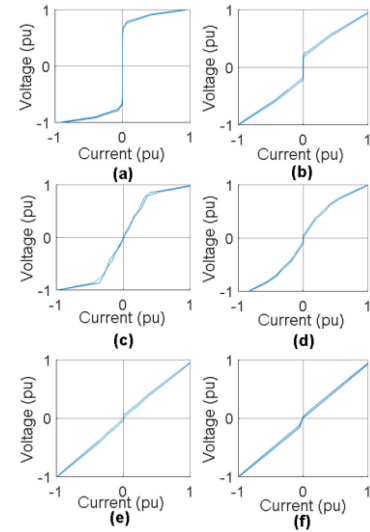Fig. 5.   HIF current characteristics.

Fig. 6.   Different HIF V-I characteristics obtained from the same HIF model resembling real-field data: (a) concrete, (b) wet grass, (c) dry tiles, (d) damp sand, (e) dry rubber, and (f) damp tiles.

to the transient analysis control (TACS) used in [40]. Finally, the variable resistors are connected to the distribution grid via single switch that produces the intermittence. In Fig. 5 we can see the HIF current characteristics with intermittence at around 0.1 s and buildup and shoulder starting at around 0.3 s.

The HIF model for IEEE-13 node distribution system has following parameters. The resistances R_n and R_p have random variation from a minimum of 1 Ω to maximum 56 Ω. The ideal diodes, D_N and D_P have resistances of 0.01 Ω and 0.001 Ω respectively. DC_N and DC_P are the DC sources with 0.10 V and 0.15 V rating respectively. The non-linearity element in the HIF model is varied to get different V-I characteristics to resemble HIF fault current for different fault surfaces as seen in Fig. 6. The HIF V-I characteristics shown in Fig. 6 are similar to those obtained from real field tests in [3] and [8].

B. Test System

IEEE-13 node and IEEE-34 node distribution test feeder systems [41] are used as test systems. The IEEE-34 node is a large distribution network with a feeder voltage rating of 24.9 kV while IEEE-13 node is a small and heavily loaded network with feeder voltage of 4.16 kV. Fig. 7 and Fig. 8 show IEEE-34 node and IEEE-13 node feeders with the placement points of the measurement devices. The measurement devices are evenly
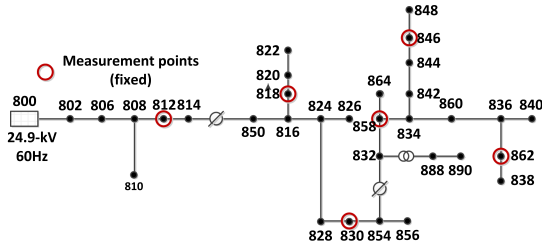
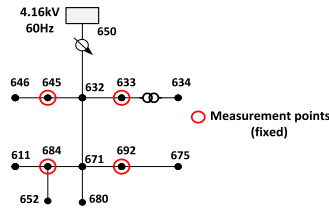Fig. 7. IEEE-34 node test distribution feeder (with measurement points).

Fig. 8. IEEE-13 node test distribution feeder (with measurement points).

spaced out throughout both the networks and their placement is fixed. The measurement device placement nodes for IEEE-34 node feeder are at nodes 812, 818, 830, 846, 858 and 862. The measurement device placement nodes for IEEE-13 node feeder are at nodes 633, 645, 684 and 692.

IV. SIMULATION CASES

ADDT should be robust enough to correctly distinguish and detect HIF from other non-harmful grid events. Hence, in the simulation cases, ADDT's functionality is validated against both, the short transient events such as capacitor and load switching and the long transient events such as motor starting and feeder energization. The short transient events are simulated for both IEEE-34 node and IEEE-13 node distribution test feeders. Since the probability of a HIF occurrence is much higher at voltage levels of 15 kV and below (see IEEE PSRC report in [1]), the additional set of simulation studies involving long transient events and a sensitivity test are simulated for IEEE-13 node feeder. In our simulation studies, we also attempt to show that dividing distribution networks in multiple zones provides better results. Such a concept is called *Grid Zoning*. Grid Zoning is explained and implemented early in the simulation cases based on short transient events and then used further for long transient events and sensitivity tests. The various simulation cases along with event placement points to asses ADDT's functionality as divided among both IEEE-34 and IEEE-13 node systems can be seen in Table II. The simulation cases pertaining to short transient events are organized as:

A. Short Transient Events

1) Robustness to False Positives:

a) Load and capacitor switching: Load and capacitor switching are the two most common events in the distribution network. They are generally planned activities and do not pose any risk to normal grid operations unlike a HIF event. Load

TABLE II
SIMULATION CASE EVENT PLACEMENT NODES

Short Transient Events				
IEEE-34 Node Test Feeder				
Simulation Case	**Scenario**	**HIF node**	**2-ϕ load node**	**3-ϕ Capacitor node**
I. Robustness to false positives	A	-	816	836
	B	-	854	834
II. Robustness to false negatives	A	854	836	816
	B	834	836	854
III. Grid Zoning	B	834	836	854
IEEE-13 Node Test Feeder				
Simulation Case	**Scenario**	**HIF node**	**2-ϕ load node**	**3-ϕ Capacitor node**
IV. Robustness to false positives (with grid zoning).	A	-	646	634
	B	-	680	671
V. Robustness to false negatives (with grid zoning).	A	675	646	634
	B	675	680	671
Long Transient Events				
IEEE-13 Node Test Feeder				
Simulation Case	**HIF node**	**Motor node**	**Feeder Energization Switch placement**	
VI. Motor Starting (with grid zoning)	675	634	-	
VII. Feeder Energization (with grid zoning)	675	-	Between node 632 and node 671	
Sensitivity Test				
IEEE-13 Node Test Feeder				
Simulation Case	**HIF Node**			
VIII. Sensitivity Test	675			

switching is a temporary event which might produce distortions in few samples of the waveform at the instant of switching but the distortions will not sustain over time and severity rating thresholds will not be violated. Capacitor switching also leads to temporary high frequency oscillatory transients causing momentary waveform distortions but the effect does not last long after the switching event is over. However, in case of HIF as seen in Fig. 5, the fault current follows the buildup and shoulder characteristics leading to increasing distortions. The intermittence characteristic of fault current would ensure that distortions sustain over time and don't die out until HIF is cleared. As explained in [8], a resistive–inductive or resistive-capacitive element have ellipse as their V-I characteristic while the HIF V-I characteristics can be seen in Fig. 6. Load or capacitor switching has the potential to mislead ADDT into identifying

them as events harmful to grid. Hence, ADDT should be robust to such false positives. This test for robustness is created by simulating both load and capacitor switching at the same time in order to increase the chance of false detection. The events are simulated for two scenarios (A and B); these scenarios differ by event placement points as shown in Table II. In scenario B, the events happen at close proximity to each other, while in scenario A the events are geographically distant from each other. Scenario B intends to have higher number of distorted samples at a closer geographical proximity which would mislead the near-by measurement devices to go up the severity scale. This increase in severity scale can mislead ADDT in deducing normal switching events as possibly harmful event. Hence, scenario B is more stringent and acts as an enhanced test of robustness of ADDT to false positives.

b) Harmonics distortion: Harmonics also have the potential to distort the waveforms. For voltage waveforms in a system below 69 kV, the IEEE standards recommend 3% distortion limit of individual harmonics and 5% Total Harmonic Distortion (THD) limit [42]. Hence, ADDT should be insensitive to harmonic distortions within prescribed limits. The test of ADDT's robustness to harmonics distortion forms Scenario C for the simulation case I.

2) Robustness to False Negatives: In this simulation case, we investigate ADDT's robustness to false negatives i.e., ADDT's ability to distinguish and detect HIF even when normal grid events like load and capacitor switching are simulated at the same time as HIF. Utilizing ADDT's severity scale, we also try to give a fair idea of HIF location. The event placement points are shown in Table II. This simulation case is also performed for two scenarios with events happening at close proximity to each other in scenario B. It is worth mentioning that scenario B represents the most challenging test of ADDT's robustness to false negatives.

3) Grid Zoning: In case of distribution grids, dividing the network into multiple zones of observation provides better situational awareness of the grid. The IEEE-34 node feeder is divided in two zones with equal number of measurement devices in each one. Zone 1 will have Common Reporting's from devices at Nodes 812, 818, 830 while Zone 2 will have Common Reporting's from devices at Nodes 858, 846, 862. Similarly, the IEEE-13 node feeder is divided into two equal zones with Zone 1 having Common Reporting's from measurement devices at Nodes 633 and 645 while Zone 2 has Common Reporting's from measurement devices at Nodes 684 and 692 respectively. The results of zone wise division would be compared against that of the Common Reporting's of the undivided network in order to illustrate the benefits of zonal division. The zoning implemented in this paper is rudimentary in nature and follows the idea of dividing the grid in equal zones for better observability and decision-making. If in IEEE-34 node feeder, a HIF occurs between nodes 830 and 858, it would be challenging for the current grid zoning scheme to accurately locate the event but the LMD level reporting can compensate for that. A high LMD level severity rating for devices at node 830 and 858 will help in detecting and locating the HIF event occurring between them. In practice, the division of distribution network into zones should

be based upon multiple factors like line length, load distribution, availability of maintenance teams etc. The ultimate decision of zoning will depend on a particular DSO and the grid network in question. Further studies would be required to devise an optimal approach for grid zoning and such investigation is outside the scope of this paper.

B. Long Transient Events

1) Robustness to Motor Starting: Motor starting is a common occurrence in distribution grids and takes longer to reach steady state than events like load or capacitor switching. Hence, in this simulation case we evaluate ADDT's robustness to motor starting. Since, majority of the dynamic loads in power systems are induction machines [43], an induction machine with parameters from [44] has been used in our simulation studies. The motor is connected at node 634 while HIF is simulated at node 675 as seen in Table II. The HIF and motor starting is simulated at the same time to increase the complexity of detection for ADDT.

2) Robustness to Feeder Energization: Feeder energization leads to transients which can be mistaken for HIF signature. Hence, in this simulation case, a switch between the nodes 632 and 671 is used. The lower half of IEEE-13 Feeder remains un-energized initially. The HIF and the switching leading to feeder energization are simulated at the same time.
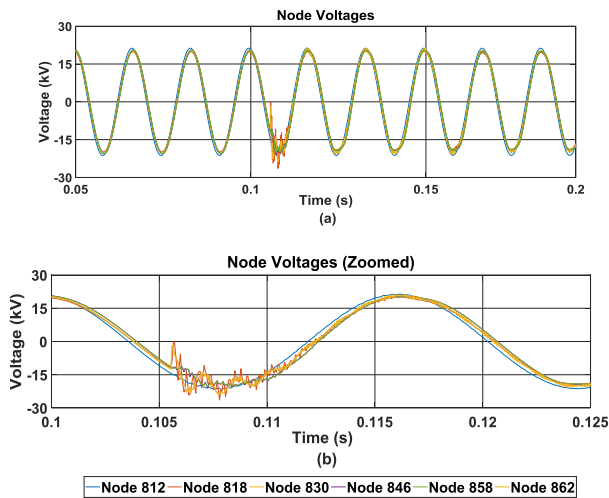
C. Sensitivity Test

ADDT performance is influenced by the waveform distortions. As summarized in [45], HIF currents and their characteristics can vary according to the fault surface. The number of distortions and the frequency of their occurrence in the monitored sinusoidal waveforms will depend on the HIF V-I characteristics. Hence, it is important and prudent to evaluate ADDT's sensitivity to different HIF V-I characteristics arising from different fault surfaces. The sensitivity test utilizes the different characteristics obtained in Fig. 6 since they resemble the data obtained from field tests. The sensitivity test is conducted for the IEEE-13 node feeder.

It should be noted that in all the simulation cases for both IEEE-34 and IEEE-13 node feeders, we use sampled (128 samples per cycle) voltage waveforms for ADDT analysis. The time-frame for re-allocation of severity rating is selected as 0.1 s. This interval of 0.1 s is also referred as reporting interval. In simulation cases of IEEE-34 node feeder, HIF is always simulated at phase A to ground. The load switching is a 2-phase unbalanced load switching between phases A-B. The capacitor bank is star grounded with capacitance of 1.2835 μF. Load and capacitor bank are switched OFF after three cycles. In simulation cases of IEEE-13 node feeder, HIF is always simulated at phase C to ground. Load switching, capacitor bank switching, motor starting, feeder energization and HIF (cases where applicable) all are triggered at $t = 0.105$ s. In case of motor starting HIF is cleared after 3 s of initiation while in case of feeder energization HIF is cleared at 1 s.

TABLE III
SIMULATION CASE II, SCENARIO B, ADDT IMPLEMENTATION RESULTS (PHASE A)

Reporting Interval	Node 812		Node 818		Node 830		Node 846		Node 858		Node 862	
	Distortions Recorded	LMD Severity Rating	Distortions Recorded	LMD Severity Rating	Distortions Recorded	LMD Severity Rating	Distortions Recorded	LMD Severity Rating	Distortions Recorded	LMD Severity Rating	Distortions Recorded	LMD Severity Rating
T1=(0.0-0.1)s	0	0	0	0	0	0	0	0	0	0	0	0
T2=(0.1-0.2)s	57	1	72	1	87	2	95	2	105	2	99	2
T3=(0.2-0.3)s	32	0	34	0	77	2	91	2	96	2	101	2
T4=(0.3-0.4)s	19	0	23	0	66	1	92	2	93	2	83	2

Fig. 9. Measured voltages at different measurement points for Simulation Case II, Scenario B. HIF event and capacitor and load switching occur at t = 0.105 s. (a) Node Voltages. (b) Node Voltages (Zoomed).

Fig. 10. Distortions detected across different measurement devices for Simulation Case II, Scenario B.

V. SIMULATION RESULTS

The simulation results are as follows:

A. Short Transient Events

We discuss in detail ADDT analysis results of the most interesting and challenging case i.e., simulation case II, scenario B. We also show the benefits of implementing grid zoning for the same. After this discussion, we provide a brief summary of results of other simulation cases.

1) IEEE-34 Node Test Feeder:

a) Simulation case II, scenario B: The complexity of this simulation case lies in the fact that the events of HIF, load and capacitor switching are simulated at close proximity to each other and at the same time in order to mislead the ADDT into mistaking HIF for a normal grid event. In Fig. 9, we can see the voltage waveforms from all measurement devices (see Fig. 7 for exact placement). The ADDT implementation results for the waveforms are shown in Table III. It can be seen that as the events are simulated, ADDT reports increased waveform distortions from all the measurement devices. Accordingly, the severity rating of the measurement devices also change. The measurement devices near the event of HIF show higher amount of distorted samples in comparison to other devices. The device at node 858 indicates a severity rating of level 2 and sustains
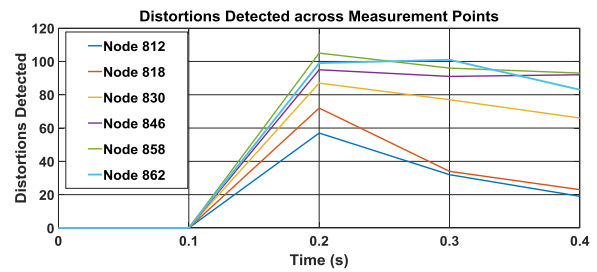
it over next three reporting interval. The devices at node 862 and 846 also show sustained high severity rating for the same reporting intervals. The device at node 830 is comparatively far from HIF event but still sustains severity rating of 2 for two time intervals possibly due to combined effect of HIF and capacitor switching. However as the effect of capacitor switching fades away, the severity rating goes a level down. Nodes 812 and 818, similarly sustain severity rating level 1 for first reporting interval but as the load switching effect fades away, the severity rating for the nodes goes to level 0. Based on these observations, the event can be classified as a potentially harmful event that is occurring somewhere between nodes 830, 846, 858 and 862. The distortions detected over time are shown graphically in Fig. 10.

b) Simulation case III, scenario B: This simulation case illustrates the benefits of grid zoning. The proposed grid zoning is implemented utilizing the ADDT results obtained from simulation case II, scenario B. The results of grid zoning can be observed in Table IV. Based on observations from Table IV; the common reporting's of the undivided network shows severity rating of level 1 only for one reporting period, as the devices far from HIF (nodes 812, 818) report too few distortions. However this is an incorrect representation of grid condition. When observing zone based data, it can be seen that Zone 1 also has severity rating level 1 for one reporting interval. It indicates that while Zone 1 is initially affected, the impact fades away quickly and severity rating goes to level 0 from level 1. However, Zone 2 remains affected throughout indicating potentially harmful event taking place in the area covered by the zone. Thus, the area of operation for maintenance teams will reduce considerably as the location of the harmful event can be narrowed down to area between devices at nodes 858, 846 and 862. This will ensure efficient dispatch of resources and quicker mitigation of the event. Fig. 11 shows the variation of Network Level severity

TABLE IV
SIMULATION CASE III, SCENARIO B (ADDT IMPLEMENTATION RESULTS OF SIMULATION CASE II, SCENARIO B WITH GRID ZONING)

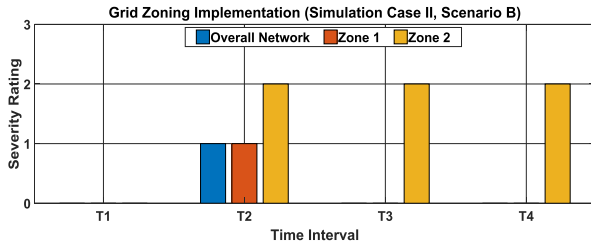| Reporting Interval	Overall Network		Zone 1 (Nodes 812, 818, 830)		Zone 2 (Nodes 846, 858, 862)	
	Common Reporting's	NT Severity Rating	Common Reporting's	NT Severity Rating	Common Reporting's	NT Severity Rating
T1=(0.0-0.1)s	0	0	0	0	0	0
T2=(0.1-0.2)s	48	1	51	1	84	2
T3=(0.2-0.3)s	21	0	22	0	89	2
T4=(0.3-0.4)s	12	0	15	0	75	2

Fig. 11.   Variation of severity ratings for different network zones with grid zoning for Simulation Case III, Scenario B.

Fig. 13.   FFT of grid voltage with injected harmonics (Simulation Case I, Scenario C).

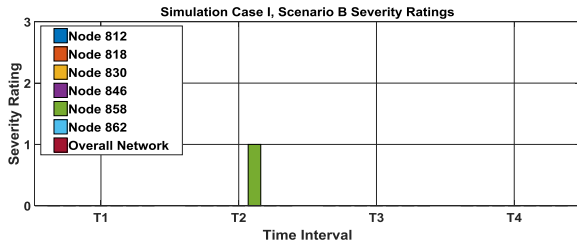Fig. 12.   Node and overall network severity rating for Simulation Case I, Scenario B.

Fig. 14.   Node and overall network severity rating for Simulation Case II, Scenario A.

ratings for different zones. Hence, ADDT analysis combined with grid zoning is effective in detecting a potentially harmful event (in this case HIF) in the grid and gives a fair idea of its location. ADDT also successfully distinguishes HIF from capacitor and load switching thereby showcasing its robustness to false negatives.

c) Simulation case I, scenario A: Simulation case I is test of ADDT's robustness to false positives. In this scenario of simulation case I, the load and capacitor switching events are distanced from each other. Based on ADDT analysis, the severity ratings of all measurement devices at different nodes and the overall network based on common reporting's don't violate the thresholds and severity ratings remain at level 0 indicating normal grid operations.

d) Simulation case I, scenario B: This case-scenario provides a tough test of ADDT's robustness to false positives. The load and capacitor switching events are close to each other. Based on ADDT analysis, the severity ratings of all measurement devices at different nodes and the severity rating of the overall network based on common reporting's are shown in Fig. 12. The measurement device at node 858 goes to level 1 indicating minimal risk while other measurement devices and overall network indicate severity rating of 0. This is on account of capacitor
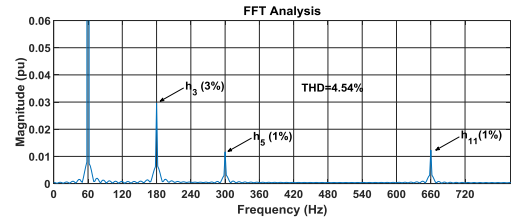
switching at node 834 but as the effect of switching fades away, severity rating of level 1 of device at node 858 is not sustained and it scales down and remains at level 0 indicating normal grid operations.

e) Simulation case I, scenario C: In this scenario, the 3rd, 5th and 11th order harmonics are injected at 3%, 1% and 1% of the fundamental frequency voltage at the power frequency of 60 Hz respectively. The total harmonic distortion (THD) stands at around 4.54%. All the harmonic values are within IEEE recommended limits. In Fig. 13, we can see the FFT analysis of the harmonic injected voltage waveform. Based on observations from ADDT analysis, we see no violation of thresholds and hence the severity rating for all the measurement points and overall network remains at level 0.

f) Simulation case II, scenario A: This simulation case and scenario is a test of ADDT's robustness to false negatives. The HIF, load and capacitor switching events are spaced out from each other. Based on ADDT analysis, severity ratings of all measurement devices and overall network are shown in Fig. 14. The devices at nodes 818, 830, 846, 858 and 862 indicate increase in severity levels. However with time, the severity rating of device at nodes 846 and node 858 sustains at level 1 while that of device at nodes 830 escalate and sustain at level two. Prima facie, the location could be zeroed down to areas between
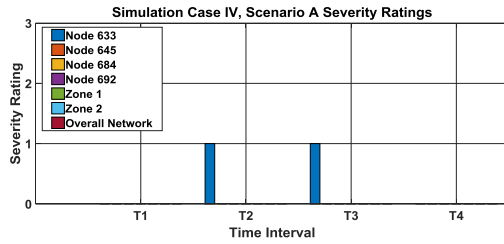
Fig. 15. Node and overall network severity rating for Simulation Case IV, Scenario A.
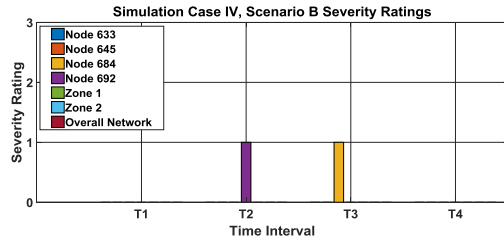

Fig. 16. Node and overall network severity rating for Simulation Case IV, Scenario B.
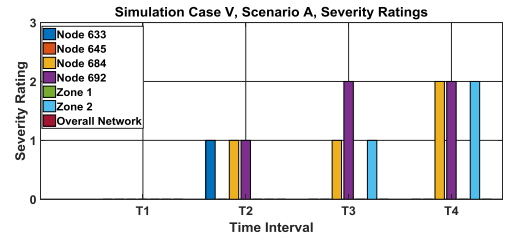

Fig. 17. Node and overall network severity rating for Simulation Case V, Scenario A.
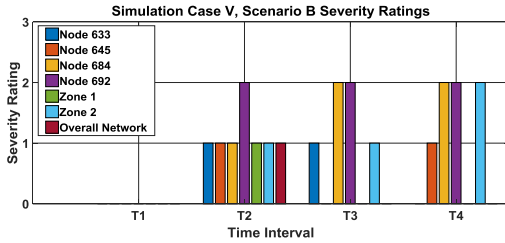

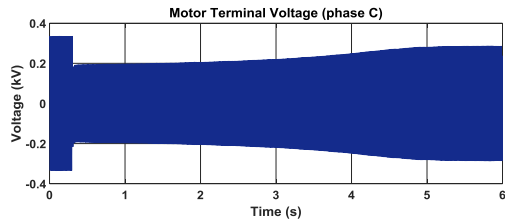Fig. 18. Node and overall network severity rating for Simulation Case V, Scenario B.

Fig. 19. Voltage at Node 634(phase C) during motor starting event.

nodes 830, 846 and 858. The severity rating for overall network, however, does not change due to devices at nodes 812, 818, and 862 hardly detecting any distortions. Hence, grid zoning as explained earlier would have provided a better representation of severity of the event to the grid operations helping achieve better decision-making.

2) IEEE-13 Node Test Feeder:

a) Simulation case IV, scenario A: This simulation case and scenario is similar to *Simulation Case I, Scenario A* with grid zoning applied. The events of load and capacitor switching are far from each other and occur simultaneously. As seen in Fig. 15, the measurement device at node 633 shows severity rating 1 for two reporting periods but other devices stay at level 0. The results from grid zoning also show no change in severity levels indicating no harm to grid operations.

b) Simulation case IV, scenario B: This simulation case and scenario is similar to *Simulation Case I, Scenario B* with grid zoning applied. The events of load and capacitor switching are closer to each other leading to measurement device at node 684 and node 692 to indicate severity level 1 for different reporting periods but the ratings of other devices and the grid zoning stay at level 0 indicating normal grid operations. The severity ratings can be seen in Fig. 16.

c) Simulation case V, scenario A: This simulation case and scenario is similar to *Simulation Case II, Scenario A* with grid zoning applied. All the three events of HIF, load and capacitor switching happen at same time but are spaced out from each other. As seen in Fig. 17, measurement devices at nodes 633, 684 and 692 indicate severity rating level 1 at different reporting periods. The severity rating of nodes 684 and 692 increases and sustains level 2 and the grid zoning results also indicate that a potentially harmful event has occurred in Zone 2.

d) Simulation case V, scenario B: This simulation case and scenario is similar to *Simulation Case II, Scenario B* with

grid zoning applied. The simulation of all the events at close proximity to each other causes severity level 1 rating across all measurement devices except at node 692. The measurement device at node 692 maintains severity level 2 throughout. As seen in Fig. 18, the grid zoning results indicate severity rating level 1 initially for the all the measurement devices, different Zones and overall network. However, in the following reporting periods, the severity rating of device at node 684 increases to severity level 2. The severity level 2 of devices at node 684 and 692 sustains leading to eventual increase of severity rating of Zone 2 to level 2 indicating a potentially harmful event occurrence in that area.

B. Long Transient Events

1) Simulation Case VI, Motor Starting: Motor starting is a phenomenon with a long transient and lasts till the motor accelerates to the full rated speed. During this time, high current is drawn and there is considerable voltage drop until slowly motor reaches a steady state of operation. ADDT's robustness against motor starting transients is evaluated in this simulation case. The motor at node 634 and HIF at node 675 are initiated at $t = 0.105$ s. The voltage at node 634 during the motor start process can be seen in Fig. 19, which lasts till almost 6 s.

The reporting period is 0.1 s. Hence there would be 60 reporting intervals for 6 s. Due to the enormity of data generated
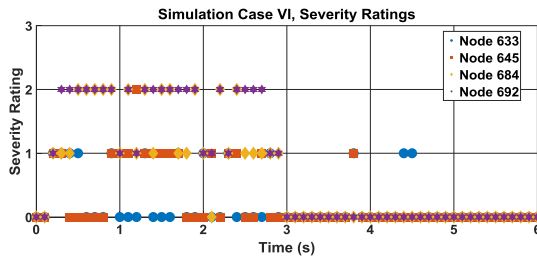
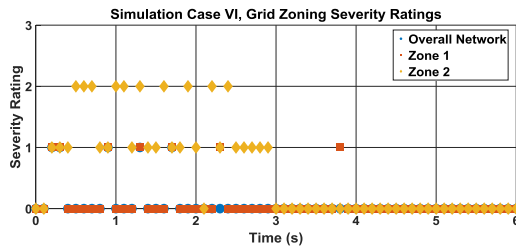Fig. 20.   Node severity ratings for Simulation Case VI.

Fig. 21.   Grid Zoning based severity ratings for Simulation Case VI.
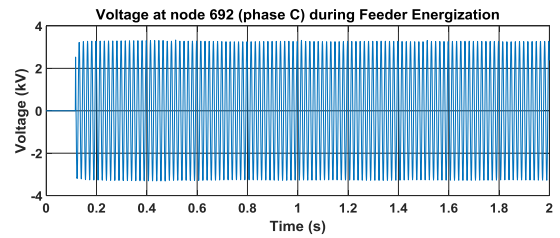

Fig. 22.   Voltage at node 692 during feeder energization event.
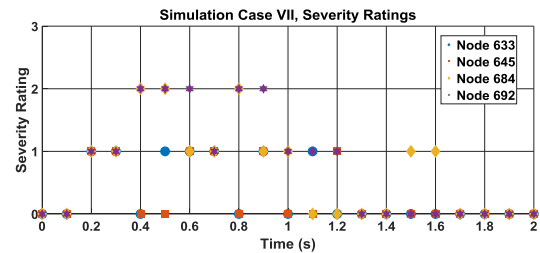

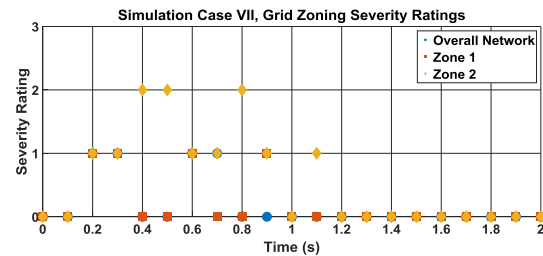
Fig. 23.   Node severity ratings for Simulation Case VII.

Fig. 24.   Grid Zoning based severity ratings for Simulation Case VII.

a concise summary of ADDT implementation results are presented via means of a scatter graphical representation in Fig. 20 and Fig. 21.

In Fig. 20, it can be observed that the device at node 692 mostly indicates level 2 rating until almost 3 s and after that it scales down to level 0. Similarly, device at node 684 indicates rating of level 1 and level 2 intermittently until 3 s. Node 645 measurements indicate level 1 for few instants and one indication of level 2 rating in the first 3 s and show one instance of level 1 around 4 s. Node 633 measurements largely remain at level 0 barring few instances of level 1 rating. The conclusion that can be drawn from these observations is that motor starting does not lead to many distortions that will violate ADDT thresholds. The amplitude of the voltage waveforms do vary as the motors attains steady state but the sinusoidal nature of the waveforms is also retained. Since, the fundamental properties of sinusoids are hardly violated during the motor start transient; it leads to very few distortions as observed in severity ratings of the closest measurement device at node 633.

In Fig. 21, the grid zoning severity ratings for simulation case VI can be observed. It can be seen that overall network remains at level 0 almost throughout the 6 s, which is misleading since a HIF event does occur. Zone 1 shows few level 1 indications during first 3 s and just one level 1 rating around 3.75 s but otherwise remains at level 0 indicating little effect from motor starting occurring in the area observed and also due to considerable distance from HIF event. Zone 2 indicates level 2 rating for several instances during the first 3 s. Zone 2 clearly indicates a potentially harmful event until 3 s (in this case HIF) in the area observed thereby highlighting the effectiveness of grid zoning.

2) Simulation Case VII, Feeder Energization: Feeder energization is another common occurrence in active distribution grids. The switches between nodes 632 and 671 are switched on simultaneously with the HIF event in node 675 at $t = 0.105$ s.

The voltage pattern recorded from the measurement device at node 692 can be observed in Fig. 22.

The severity levels for the different measurement devices at different nodes can be seen in Fig. 23. Devices at nodes 633 and 645 indicate few instances of level 1 rating mostly until 1 s and then scale down to level 0. The fact that this zone of feeder is already energized and there is considerable distance from the HIF event leads to few distortions. Device at node 684 mostly remains at level 1 with few instances of level 2 rating during the first 1 s. However, it scales to level 1 on three different instances after 1 s probably on account of distortions produced due to feeder energization. Device at node 692 gradually scales up and subsequently maintains level 2 for major portion of the first 1 s. Afterwards it scales down to level 0 barring two instances. The feeder energization event produces few and far between distortions which does not lead to consistent violation of ADDT thresholds for high severity levels which becomes more evident as HIF event is cleared at 1 s.

In Fig. 24, it can be observed that Zone 2 intermittently maintains level 2 and level 1 rating during the first 1 s in comparison to Zone 1 or overall network severity ratings. Hence, one can easily deduce the possibility of a potentially harmful event occurring in Zone 2 and investigate further in that area.
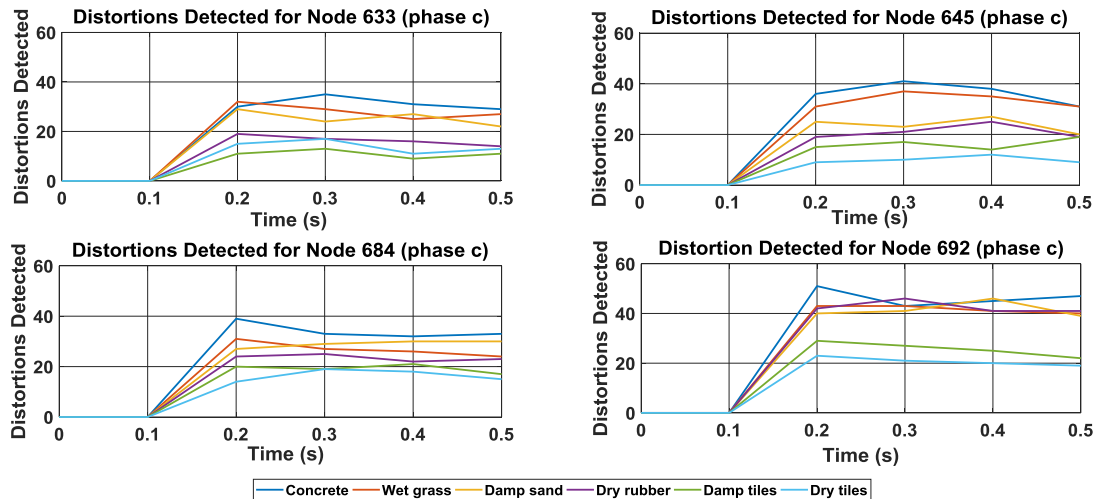
Fig. 25. Simulation Case VIII, Sensitivity Test. Distortions detected across different nodes for different HIF V–I characteristic for different fault surfaces.

C. Simulation Case VIII, Sensitivity Test

HIF currents from different surfaces are used to conduct the sensitivity test. The distortions detected over a time period of 0.5 s for measurement devices at different nodes compared against different HIF event currents simulated on node 675 at 0.105 s are shown in Fig. 25.

As observed from Fig. 25, the measurement device at node 692 records higher number of distortions for almost all HIF fault surfaces in comparison to other nodes mainly because it is closest to the event location at node 675. The distortions recorded across all nodes show maximum value for HIF fault surface of concrete. This could be attributed to the fact that V-I characteristic for concrete in Fig. 6 is quite flat near zero implying low impedance and subsequently high fault current. The distortions recorded for surfaces of wet grass, dry rubber and damp sand are similar for all the nodes except node 645 where distortions for wet grass are higher. The distortions recorded for damp and dry tiles show least amount of distortions. The difference can be more clearly observed in node 692 and node 645 recordings. The low amount of distortions correlates to weak fault current which can also be ascertained from the fact that the V-I characteristics for both damp and dry tiles are rather steep and not very flat near zero. Such weak fault current will lead to very few common reporting's in NT level severity rating which might cause ADDT not to classify the event as harmful. LMD level severity ratings of nodes 684 and 692 can help overcome such an eventuality but nodes 684 and 692 almost report same number of distortions. Such a situation will increase the area to be surveyed by maintenance team. Hence, a weak HIF can lead to comparatively higher resource and time consumption to locate the event even if the HIF is successfully detected with ADDT implementation.

However, more such case studies with real field data would be required to conduct an exhaustive evaluation of ADDT's robustness to weak HIFs. The severity level ratings structure is currently quite simple. A more robust approach would be to broaden the severity level ratings table to create subsections within each level to better classify the distortions and better accommodate weak HIFs. In order to guarantee success, such an exercise would need to be performed in close collaboration with DSO operators using the network specific data and measurements of extensive field-staged HIFs.

VI. DISCUSSIONS

In this section, based on the obtained results, we would like to compare the performance of ADDT with other HIF detection methods in literature. As established before, HIFs by nature are random and unpredictable. Algorithms in [11]–[13], [15], [24], [25] are reliant on certain harmonic components or the variation of energy of harmonic components of fault current for HIF detection. However as stated in [8] stable HIFs have limited harmonic components which are not always enough to be leveraged for detection. Algorithms in [18], [20], [22]–[23] use a wavelet approach, where the choice of mother wavelet might lead to different results since all HIFs will not always follow same patterns (as seen in Fig. 6). In comparison, ADDT leverages the sinusoid waveform distortions. Waveform distortions can be defined as persistent deviation from sinusoidal nature of the waveforms [46]. These distortions can be the consequence of events ranging from a normal capacitor switching to HIF to three-phase faults. However, the number and frequency of distortions would vary according to the event. Utilizing a system of indicators and thresholds, ADDT distinguishes HIF from other normal grid events. In this paper, ADDT's robustness had been rigorously assessed by subjecting it to a series of complex tests including simultaneous occurrence of HIF with other grid events, the likes of which has been conducted for few cases only in [21]. Due to the random nature of HIF, ADDT's detection sensitivity to HIFs on different surfaces has also been evaluated. Considering the first reporting of severity level 2 as an indicator of HIF, the performance of ADDT is comparable or faster than the fast HIF detection methods in [2], [16]. The concept of severity rating scale and grid zoning for ADDT has been introduced for the first time in this paper.

The concept of severity scale and grid zoning are aimed to provide a refined understanding of the event metrics to the control room operators in order to better classify and locate the event. Implementation of a wavelet, Fourier or neural network based technique would require higher computing power. In comparison, ADDT has low computational burden which makes its implementation faster and easier. ADDT however is sensitive to correct determination of thresholds and severity levels as a misalignment could potentially lead to incorrect classification and wrong results. That being said, ADDT is very flexible since most of the parameters are user-dependent which can be adjusted according to grid requirements and can be systematically improved over time.

VII. CONCLUSION

This paper presents the implementation of ADDT to detect HIF in IEEE-34 and IEEE-13 node distribution test feeder systems. The sampled voltage waveforms from different parts of the distribution grid were monitored by ADDT in real-time and the violation of pre-determined thresholds coupled with information from pre-defined indicators was used for classification of the event causing the violations. Classification also indicated the severity of the event causing violations and its possible location. The simulation cases were devised with different scenarios mimicking realistic grid conditions to evaluate ADDT for both short and long transients. The ADDT analysis for the different simulation cases shows its ability to distinguish and detect HIF in spite of false negatives and its robustness to false positives, thereby highlighting the efficiency and reliability of ADDT. A sensitivity test is also conducted to evaluate ADDT performance for HIF with different distortions due to different fault surfaces.

Since, the simulation cases devised and models designed in this paper were in a laboratory setup, future work will evaluate ADDT in field-staged HIF conditions (an interesting study case can be an HIF caused by tree contact where the overhead line remains unbroken). The operation of nonlinear loads along with HIF will be explored in future work to investigate ADDT's robustness under a different angle. Optimal placement of measurement points according to the grid topology to capture relevant event signatures is another area where progress can be made. Reliability of ADDT in power grids with considerable penetration of distributed generation should be also investigated. Finally, the application of ADDT is not restricted to HIF detection only and it will be further enhanced to detect other potential grid disrupting events which remain undetected by conventional protection systems.

REFERENCES

[1] "High impedance fault detection technology," Mar. 1996. Report of PSRC Working Group D15. [Online]. Available: http://www.pes-psrc.org/kb/published/reports/High_Impedance_Fault_Detection_Technology.pdf

[2] S. Gautam and S. M. Brahma, "Detection of high impedance fault in power distribution systems using mathematical morphology," *IEEE Trans. Power Syst.*, vol. 28, no. 2, pp. 1226–1234, May 2013.

[3] A. Sultan, "Detecting arcing downed-wires using fault current flicker and half-cycle asymmetry," *IEEE Trans. Power Del.*, vol. 9, no. 1, pp. 461–470, Jan. 1994.

[4] J. Carr, "Detection of high impedance faults on multi-grounded primary distribution systems," *IEEE Trans. Power Appl. Syst.*, vol. PAS-100, no. 4, pp. 2008–2016, Apr. 1981.

[5] R. Lee and M. Bishop, "Performance testing of the ratio ground relay on a four-wire distribution feeder," *IEEE Trans. Power Appl. Syst.*, vol. PAS-102, no. 9, pp. 2943–2949, Sep. 1983.

[6] B. D. Russell and C. L. Benner, "Analysis of high impedance faults using fractal techniques," *IEEE Trans. Ind. Appl.*, vol. 33, no. 3, pp. 635–640, May/Jun. 1997.

[7] C. J. Kim and B. D. Russell, "Analysis of distribution disturbances and arcing faults using the crest factor," *Elect. Power Syst. Res.*, vol. 35, pp. 141–148, 1995.

[8] B. Wang, J. Geng, and X. Dong, "High-impedance fault detection based on nonlinear voltage–current characteristic profile identification," *IEEE Trans. Smart Grid*, vol. 9, no. 4, pp. 3783–3791, Jul. 2018.

[9] I. Zamora, "New method for detecting low current faults in electrical distribution systems," *IEEE Trans. Power Del.*, vol. 22, no. 4, pp. 2072–2079, Oct. 2007.

[10] M. Aucoin and B. D. Russell, "Detection of distribution high impedance faults using burst noise signals near 60 Hz," *IEEE Trans. Power Del.*, vol. 2, no. 2, pp. 342–348, Apr. 1987.

[11] D. I. Jeerings and J. R. Linders, "Unique aspects of distribution system harmonics due to high impedance ground faults," *IEEE Trans. Power Del.*, vol. 5, no. 2, pp. 1086–1094, Apr. 1990.

[12] K.-Y. Lien, "Energy variance criterion and threshold tuning scheme for high impedance fault detection," *IEEE Trans. Power Del.*, vol. 14, no. 3, pp. 810–817, Jul. 1999.

[13] S. M. Shahrtash and M. Sarlak, "High impedance fault detection using harmonics energy decision tree algorithm," in *Proc. Int. Conf. Power Syst. Technol.*, Chongqing, 2006, pp. 1–5.

[14] A. Emanuel, "High impedance fault arcing on sandy soil in 15 kV distribution feeders: contributions to the evaluation of the low frequency spectrum," *IEEE Trans. Power Del.*, vol. 5, no. 2, pp. 676–686, Apr. 1990.

[15] D. Jeerings and J. Linders, "A practical protective relay for down-conductor faults," *IEEE Trans. Power Del.*, vol. 6, no. 2, pp. 565–574, Apr. 1991.

[16] É. M. Lima, C. M. dos Santos Junqueira, N. S. D. Brito, B. A. de Souza, R. de Almeida Coelho, and H. Gayoso Meira Suassuna de Medeiros, "High impedance fault detection method based on the short-time Fourier transform," *IET Gener., Transmiss. Distrib.*, vol. 12, no. 11, pp. 2577–2584, 19 6 2018.

[17] D. C. T. Wai and X. Yibin, "A novel technique for high impedance fault identification," *IEEE Trans. Power Del.*, vol. 13, no. 3, pp. 738–744, Jul. 1998.

[18] T. Lai, "High-impedance fault detection using discrete wavelet transform and frequency range and rms conversion," *IEEE Trans. Power Del.*, vol. 20, no. 1, pp. 397–407, Jan. 2005.

[19] N. Elkalashy, "Modeling and experimental verification of high impedance arcing fault in medium voltage networks," *IEEE Trans. Dielect. Elect. Insul.*, vol. 14, no. 2, pp. 375–383, Apr. 2007.

[20] M. F. Akorede and J. Katende, "Wavelet transform based algorithm for high- impedance faults detection in distribution feeders," *Eur. J. Sci. Res.*, vol. 41, no. 2, pp. 238–248, 2010.

[21] W. C. Santos, F. V. Lopes, N. S. D. Brito, and B. A. Souza, "High-Impedance fault identification on distribution networks," *IEEE Trans. Power Del.*, vol. 32, no. 1, pp. 23–32, Feb. 2017.

[22] A.-R. Sedighi, "High impedance fault detection based on wavelet transform and statistical pattern recognition," *IEEE Trans. Power Del.*, vol. 20, no. 4, pp. 2414–2421, Oct. 2005.

[23] H. Jabr and A. Megahed, "A wavelet-FIRANN technique for high-impedance arcing faults detection in distribution systems," in *Proc. Int. Conf. Power Syst. Transients (IPST05)*, Jun. 2005, pp. 1–6.

[24] S. R. Samantaray and P. K. Dash, "High impedance fault detection in distribution feeders using extended Kalman filter and support vector machine," *Eur. Trans. Elect. Power*, vol. 20, no. 3, pp. 382–393, Apr. 2010.

[25] A. Girgis, "Analysis of high-impedance fault generated signals using a Kalman filtering approach," *IEEE Trans. Power Del.*, vol. 5, no. 4, pp. 1714–1724, Oct. 1990.

[26] C. J. Kim and B. D. Russell, "Classification of faults and switching events by inductive reasoning and expert system methodology," *IEEE Trans. Power Del.*, vol. 4, no. 3, pp. 1631–1637, Jul. 1989.

[27] B. D. Russell and C. L. Benner, "Arcing fault detection for distribution feeders: Security assessment in long term field trials," *IEEE Trans. Power Del.*, vol. 10, no. 2, pp. 676–683, Apr. 1995.

[28] M. Sarlak and S. M. Shahrtash, "High-impedance faulted branch identification using magnetic-field signature analysis," *IEEE Trans. Power Del.*, vol. 28, no. 1, pp. 67–74, Jan. 2013.

[29] H. K. Zadeh, "ANN-based high impedance fault detection scheme: Design and implementation," *Int. J. Emerg. Elect. Power Syst.*, vol. 4, no. 2, pp. 1–14, 2005.

[30] S. Samantaray, "High impedance fault detection in power distribution networks using time-frequency transform and probabilistic neural network," *IET Gener. Transm. Distrib.*, vol. 2, no. 2, pp. 261–270, Mar. 2008.

[31] S. Ebron, D. L. Lubkeman, and M. White, "A neural network approach to the detection of incipient faults on power distribution feeders," *IEEE Trans. Power Del.*, vol. 5, no. 2, pp. 905–914, Apr. 1990.

[32] M. Michalik, "New ANN-based algorithms for detecting HIFs in multi-grounded MV networks," *IEEE Trans. Power Del.*, vol. 23, no. 1, pp. 58–66, Jan. 2008.

[33] C. Benner and B. Russell, "Practical high-impedance fault detection on distribution feeders," *IEEE Trans. Ind. Appl.*, vol. 33, no. 3, pp. 635–640, May/Jun. 1997.

[34] M. Yang, "Detection of downed conductor in distribution system," in *Proc. IEEE Power Eng. Soc. General Meeting*, 2005, vol. 2, pp. 1107–1114.

[35] L. Garcia-Santander, P. Bastard, M. Petit, I. Gal, E. Lopez, and H. Opazo, "Down-conductor fault detection and location via a voltage based method for radial distribution networks," *IEE Proc. - Gener., Transmiss. Distrib.*, vol. 152, no. 2, pp. 180–184, 4, March 2005.

[36] M. Sedighizadeh, "Approaches in high impedance fault detection—A chronological review," *Adv. Elect. Comput. Eng.*, vol. 10, no. 3, pp. 114–128, 2010.

[37] R. Bhandia, J. J. Chavez, M. Cvetkovic, and P. Palensky, "High impedance fault detection in real-time and evaluation using hardware-in-loop testing," in *Proc. IECON 2018 - 44th Annu. Conf. IEEE Ind. Electron. Soc.*, D.C., DC, USA, 2018, pp. 182–187.

[38] R. Bhandia, M. Cvetković, and P. Palensky, "Improved grid reliability by robust distortion detection and classification algorithm," in *Proc. IEEE PES Innovative Smart Grid Technol. Conf. Europe (ISGT-Europe)*, Sarajevo, 2018, pp. 1–6.

[39] D. Sabolic, "On the distribution network narrowband noise statistics," *Power Del. IEEE Trans.*, vol. 18, no. 1, pp. 66–68, 2003.

[40] S. R. Nam, J. K. Park, Y. C. Kang, and T. H. Kim, "A modeling method of a high impedance fault in a distribution system using two series time-varying resistances in EMTP," in *Proc. Power Eng. Soc. Summer Meeting. Conf. Proc. (Cat. No.01CH37262)*, Vancouver, BC, Canada, 2001, pp. 1175–1180, vol. 2.

[41] K. P. Schneider *et al.*, "Analytic considerations and design basis for the IEEE distribution test feeders," *IEEE Trans. Power Syst.*, vol. 33, no. 3, pp. 3181–3188, May 2018.

[42] *IEEE Recommended Practice and Requirements for Harmonic Control in Electric Power Systems*, IEEE Std 519-2014, pp. 1–29, Jun. 11, 2014.

[43] T. Thiringer and J. Luomi, "Comparison of reduced-order dynamic models of induction machines," *IEEE Trans. Power Syst.*, vol. 16, no. 1, pp. 119–126, Feb. 2001.

[44] P. Kundur, *Power System Stability and Control*. New York: McGraw-Hill, 1994.

[45] B. M. Aucoin and R. H. Jones, "High impedance fault detection implementation issues," *IEEE Trans. Power Del.*, vol. 11, no. 1, pp. 139–148, Jan. 1996.

[46] "IEEE working group on power quality data analytics," Tech. Rep. Draft report: Electrical signatures of power equipment failures. Dec. 2018. [Online] Available: http://grouper.ieee.org/groups/td/pq/data/

Rishabh Bhandia (Member, IEEE) received the B.Tech. degree in electrical and electronics engineering from Sikkim Manipal University, Gangtok, India, in 2011, and the M.S. degree in smart grid and buildings from Institut Polytechnique de Grenoble, Grenoble, France, in 2015. He is currently working toward the Ph.D. degree with the Electrical Sustainable Energy Department, Delft University of Technology, Delft, The Netherlands. His research interests include development of intelligent algorithm for failure anticipation and diagnosis in power distribution systems via real-time monitoring.

Jose de Jesus Chavez (Member, IEEE) received the M.Sc. and Ph.D. degrees from the Center for Research and Advanced Studies of the National Polytechnic Institute (CINVESTAV-IPN-Guadalajara), in 2006 and 2009, respectively. He was a Visiting Ph.D. Student in the Real-Time Experimental Laboratory (RTX-LAB) with the University of Alberta in 2009. He was a Professor with the Technological Institute of Mexico campus Morelia (ITM-Morelia) from 2010 to 2016. He joined the Intelligent Electrical Power grids group with the Delft University of Technology, Delft, as a Postdoctoral from 2016 to 2019. He is currently with the National Technological Institute of Mexico (TecNM-Morelia) as a Research Professor. His research interest includes electromagnetic transients, wide area protection, local area protection, and real-time simulation.

Miloš Cvetković received the B.Sc. degree in electrical engineering from the University of Belgrade, Belgrade, Serbia, in 2008, and the M.Sc. and Ph.D. degrees in electrical and computer engineering from Carnegie Mellon University, Pittsburgh, PA, USA, in 2011 and 2013, respectively. He is an Assistant Professor with the Electrical Sustainable Energy Department, Delft University of Technology, Delft, The Netherlands. For a period of time, he worked as a Postdoctoral Researcher in the Active-Adaptive Control Laboratory with Massachusetts Institute of Technology.. His research interests include development of co-simulations for energy grids and modeling for control and optimization of the electricity grids.

Peter Palensky (Senior Member, IEEE) received the M.Sc. degree in electrical engineering and the Ph.D. and Habilitation degrees from the Vienna University of Technology, Vienna, Austria, in 1997, 2000, and 2015, respectively. He cofounded a Envidatec, a German startup on energy management and analytics, and joined the Lawrence Berkely National Laboratory, CA, as Researcher, and the University of Pretoria, South Africa, in 2008. In 2009, he became appointed the Head of Business unit on sustainable building technologies with the Austrian Institute of Technology (AIT), and later the first Principle Scientist for complex energy systems at the AIT. In 2014, he was appointed a Full Professor for intelligent electric power grids with TU Delft. He is an active member in international committees like ISO or CEN and serves as an IEEE IES AdCom member-at-large in various functions for the IEEE. His main research fields are energy automation networks, smart grids, and modeling intelligent energy systems. He is an Editor-in-Chief for the IEEE INDUSTRIAL ELECTRONICS MAGAZINE, an Associate Editor for several other IEEE publications, and regularly organizes IEEE conferences.